



# Hybrid effect of an in situ multilayer Zn–ZnO–Cr<sub>2</sub>O<sub>3</sub> electrodeposited nanocomposite coatings for extended application

O. S. I. Fayomi, A. P. I. Popoola & A. A. Daniyan

To cite this article: O. S. I. Fayomi, A. P. I. Popoola & A. A. Daniyan (2016): Hybrid effect of an in situ multilayer Zn–ZnO–Cr<sub>2</sub>O<sub>3</sub> electrodeposited nanocomposite coatings for extended application, Particulate Science and Technology, DOI: [10.1080/02726351.2016.1163305](https://doi.org/10.1080/02726351.2016.1163305)

To link to this article: <http://dx.doi.org/10.1080/02726351.2016.1163305>



Accepted author version posted online: 22 Mar 2016.  
Published online: 22 Mar 2016.



Submit your article to this journal [↗](#)



Article views: 20



View related articles [↗](#)



View Crossmark data [↗](#)

## Hybrid effect of an in situ multilayer Zn–ZnO–Cr<sub>2</sub>O<sub>3</sub> electrodeposited nanocomposite coatings for extended application

O. S. I. Fayomi<sup>a,b</sup>, A. P. I. Popoola<sup>a</sup>, and A. A. Daniyan<sup>c</sup>

<sup>a</sup>Department of Chemical, Metallurgical and Materials Engineering, Tshwane University of Technology, Pretoria, South Africa; <sup>b</sup>Department of Mechanical Engineering, Covenant University, Ota, Ogun State, Nigeria; <sup>c</sup>Engineering Materials Development Institute, Akure, Ondo State, Nigeria

### ABSTRACT

Multifunctional composite coatings of Zn–ZnO–Cr<sub>2</sub>O<sub>3</sub> were deposited electrolytically on prepared carbon mild steel (CS) from Zn electrolyte, having Zn<sup>2+</sup> ions and uniformly dispersed nano ZnO–Cr<sub>2</sub>O<sub>3</sub> particulates. The corrosion resistance characteristics of the deposited coatings were evaluated using the linear polarization measurement method in 3.65% NaCl. The microstructural properties of the produced multilayered coatings were evaluated by scanning electron microscope (SEM) equipped with an energy dispersive spectrometer (EDS), x-ray diffraction (XRD), and atomic force microscope (AFM). Thermal deformations were observed after 4 h at 250°C and the mechanical response of the coated samples was investigated using a diamond-based Dura Scan microhardness tester and a MTR-300dry abrasive wear tester. From the results, a significant improvement in the corrosion performance of coatings was observed with bath containing less than 2 g/L. The microhardness, thermal stability, and anti-wear properties of Zn–ZnO–Cr<sub>2</sub>O<sub>3</sub> shows improved performance against Zn–ZnO coating matrixes, which was attributed to dispersive strengthening effect and grain induced effect of the ZnO/Cr<sub>2</sub>O<sub>3</sub> particulate.

### KEYWORDS

Microstructure; multilayer; nano-particles; particle characterization; thermal treatment

### Introduction

Steel is the most commonly employed metallic material in open-air structures and is used to make a range of equipment and metallic structures due to its low cost and good mechanical strength. Nevertheless, it reacts easily in ordinary moisture-containing environments (Munoz et al. 2004; Burubai and Dagogo 2007; Popoola, Fayomi, and Popoola 2012; Shukla, Singh, and Quraishi 2012). Corrosion plays a very vital role in different fields of industry and, consequently, in economics. Therefore, the protection of metals and alloys is of particular interest. Corrosion scientists and engineers are continually seeking for techniques and methods to effectively combat corrosion by learning the phenomenon and its control with the aim of finding better ways of using engineering materials. Surface enhancement of engineering materials is necessary for preventing service failures and corrosion attack in industry (Rahman et al. 2009). Zinc coatings add corrosion resistance to steel in several ways. As a barrier layer, a continuous zinc coating separates the steel from the corrosive environment. By galvanic protection, zinc acts as a sacrificial anode to protect the underlying steel at voids, scratches, and cut edges of the coating. The sacrificial properties of zinc can be seen in a galvanic series where the potential of zinc is less noble than steel in most environments at ambient temperatures. Zinc, like all metals, corrodes when exposed to the atmosphere. However, because of its ability to form dense, adherent corrosion by-products, the rate of corrosion is considerably lower than ferrous materials (10 – 100

times slower depending on the environment). Zinc corrosion products develop naturally on the surface as the coating is exposed to natural wet and dry cycles in the atmosphere and are often referred to as the zinc patina. The zinc patina acts as an additional barrier between the steel and the environment. The zinc coating can take as long as 2 years to weather completely, depending on the environment. For purposes of determining the stage of weathering, it is also called the zinc patina development (zinc oxides, zinc hydroxides, and zinc carbonate) (Shalaby et al. 1996; Harris, Mishon, and Hebron 2006; Fayomi et al. 2011).

With limitation to advanced protection of zinc properties, Zn nanocomposite coatings exhibit enhanced Zn self-healing properties, good thermal stability, and wear resistance. The excellent surface properties exhibited by Zn composite coatings are ascribed to the strengthening effect of the reinforcement materials incorporated. Materials such as Al<sub>2</sub>O<sub>3</sub>, SiO<sub>2</sub>, CeO<sub>2</sub>, ZrO<sub>2</sub>, TiO<sub>2</sub> have been used to reinforce Zn matrix for improved performance (Fayomi, Popoola, and Aigbodion 2014).

The integration of Cr<sub>2</sub>O<sub>3</sub> into Zn-rich electrolyte is very little in literature, and the only accessible effort is on Ni matrix. These particles were reported to absolutely control the thermal stability, hardness, and tribological characteristics of Ni matrix. Unfortunately, their inclusion yielded no noteworthy outcome on the corrosion (Malatji et al. 2016). Therefore, this work reports on the development and fabrication of novel Zn nanocomposite coatings reinforced with nano-sized ZnO and Cr<sub>2</sub>O<sub>3</sub> particles.

## Experimental procedure

### Preparation of substrate

Steel specimens of dimensions 30 mm × 20 mm × 1 mm were used as the substrate, and zinc sheets of dimensions 40 mm × 30 mm × 2 mm were prepared as the anodes. The initial surface preparation was performed using progressively finer grades of emery paper, as described in our earlier publications (Fayomi et al. 2011; Popoola, Fayomi, and Popoola 2012). The samples were properly cleaned with sodium carbonate, pickled, and activated with 5% HCl at ambient temperature for 10 sec, followed by instant rinsing in deionized water. The specimens were obtained from Metal Sample site in Nigeria. The chemical composition of the sectioned samples analyzed on a spectrometer was C 0.15%, Mn 0.45%, Si 0.18%, P 0.01%, S 0.031%, Al 0.005%, Ni 0.008%, Fe balance.

### Formation of deposited coating

The steel substrates were actuated by dipping into 10% HCl solution for 10 sec followed by rinsing in distilled water. Analytical grade chemicals and distilled water were used to prepare the plating solution at room temperature. The formulations were stirred for 1 day while heated at 40°C to allow for dissolution of any agglomerate in the bath solution. The bath produced

**Table 1.** Bath composition of Zn–ZnO–Cr<sub>2</sub>O<sub>3</sub> alloy co-deposition matrix.

Composition	Mass concentration (g/L)
ZnSO <sub>4</sub> ·7H <sub>2</sub> O	70
Cr <sub>2</sub> O <sub>3</sub>	8–16
ZnO	8
Boric acid	5
Glycine	5
Thiourea	5
Temperature	40°C
pH	4.5
Time	15 min
Current density	1.0 A/cm <sup>2</sup>

from the formulation shown in Table 1 was concurrently stirred and heated for several hours before plating.

### Preparation of the coatings

The prepared Zn–ZnO–Cr<sub>2</sub>O<sub>3</sub> composite bath was heated for 2 h and stirred intermittently to obtain a clear solution before it was prepared for electrolytic deposition on the steel. The prepared cathodes and anodes were connected to the DC power supply through a rectifier as presented in Figure 1. Deposition was carried out at varying applied current density of around 1.0 A/cm<sup>2</sup> for 15 min.

The distance between the anode and the cathode and the immersion depth were kept constant. Thereafter, the samples were rinsed in water and then dried. The formulated design plan for the coating is described in Table 2.

### Structural characterization of the coatings

The structural studies and elemental analysis of the fabricated alloy samples were verified using a TESCAN scanning electron microscope (SEM) with an attached energy dispersive spectrometer (EDS), and an optical microscope (OM). The phase property was observed with the help of an x-ray diffractogram. The adhesion profile, topography, and morphology of the coating were observed with the help of atomic force microscope (AFM). A high optic diamond-based Dura Scan microhardness tester was used to estimate the average microhardness of the deposit in an equal interval range.

### Thermo/electrochemical test

Isothermal heat treatment (in a direct-fired furnace atmosphere) of the Zn–ZnO–Cr<sub>2</sub>O<sub>3</sub> composite coating samples was carried out at 250°C for 6 h to check the mechanical stability of the coating. The electrochemical studies were performed

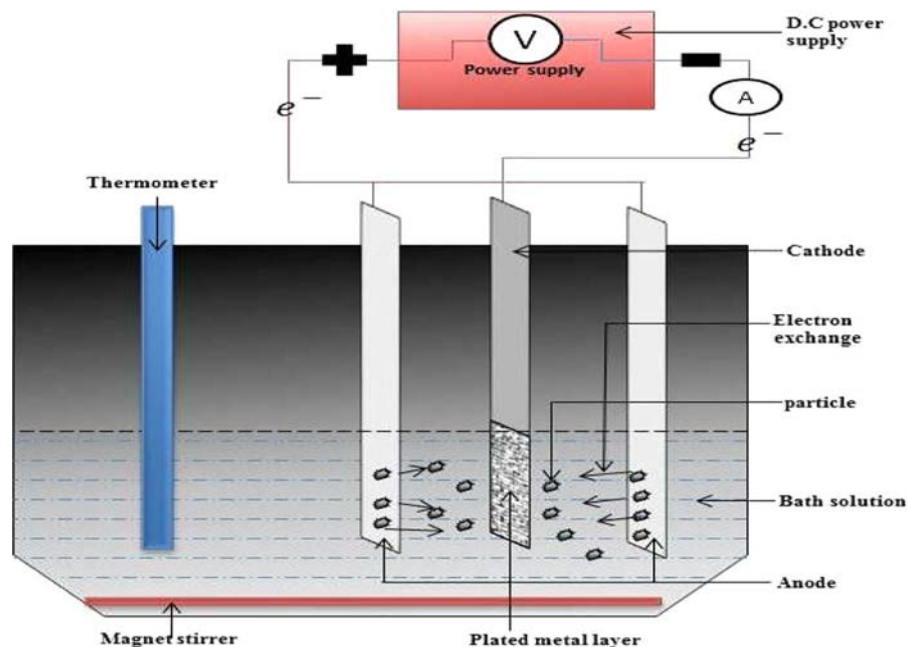


**Figure 1.** Schematic diagram of electrodeposited system.

**Table 2.** Formulated designed bath composition of Zn–ZnO–Cr<sub>2</sub>O<sub>3</sub>.

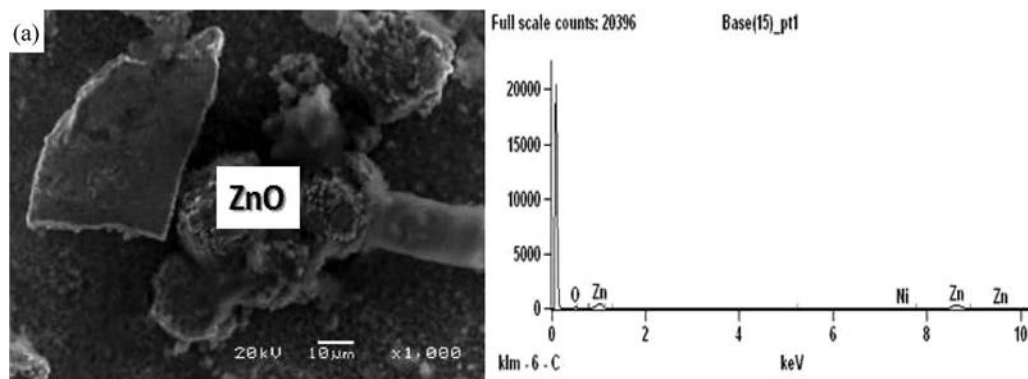
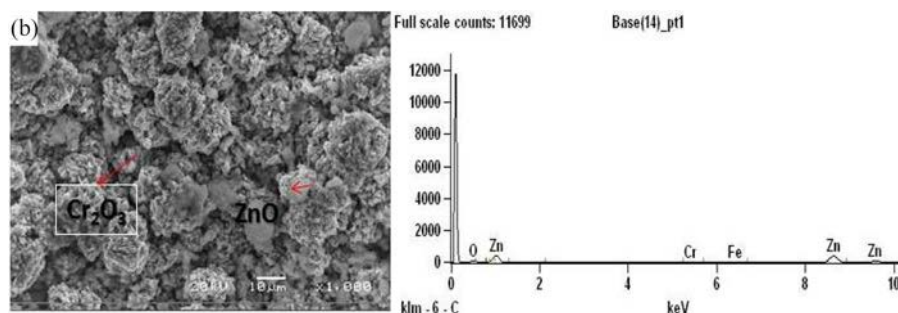
Sample order	Matrix sample	Time of deposition (min)	Current density (A/cm <sup>2</sup> )
1	Zn–8ZnO	15	1.0
2	Zn–8ZnO–8Cr <sub>2</sub> O <sub>3</sub>	15	1.0
3	Zn–8ZnO–12Cr <sub>2</sub> O <sub>3</sub>	15	1.0
4	Zn–8ZnO–16Cr <sub>2</sub> O <sub>3</sub>	15	1.0

with Autolab PGSTAT 101 Metrohm Potentiostat using a three-electrode cell assembly in a 3.65% NaCl static solution at 40°C. The developed composite was the working electrode, a platinum electrode was used as counter-electrode and Ag/AgCl was used as the reference electrode. The anodic and cathodic polarization curves were recorded at a constant scan rate of 0.012 V/sec which was fixed from  $\pm 1.5$  mV. From the Tafel corrosion analysis, the corrosion rate, potential and linear polarization resistance values were obtained.

## Results

### Surface morphology

Figures 2 and 3 show the SEM images with EDS patterns of the surfaces of the Zn–8ZnO and Zn–8ZnO–16gCr<sub>2</sub>O<sub>3</sub> composite coatings. The EDS pattern of the composite coating confirms the crystalline phase of the film. The nanoparticulates were found to be agglomerated when analyzed by SEM studies (Figure 1a). This is due to the high surface energy of the particles. In general, it can be seen that the coating on the mild steel plate resulted into a good appearance, better plating, and good adhesion.

**Figure 2.** SEM/EDS images of the Zn–8ZnO composite coating.**Figure 3.** SEM/EDS images of the Zn–8ZnO–16gCr<sub>2</sub>O<sub>3</sub> composite coating.

### XRD analysis

X-ray diffraction (XRD) patterns obtained on the electrodeposition of the composite coating is given in Figure 5, where all phases present in the matrix are clearly shown. This further confirmed the polycrystallinity of the coating particulate. From the pattern, visible phases were seen with generation of intermetallic growth, like Zn, ZnCr<sub>2</sub>, Zn<sub>2</sub>Cr<sub>7</sub>, ZnOCr<sub>2</sub> were present.

### Wear analysis of the composite coating on mild steel

Figure 6 shows the wear loss of Zn–ZnO coating and Zn–ZnO–Cr<sub>2</sub>O<sub>3</sub> composite coatings with different Cr<sub>2</sub>O<sub>3</sub> contents. It is obvious that the wear resistance of the composite coatings is more than that of Zn–ZnO coating. Although the wear resistance of the composite coatings did not increase with increase in the Cr<sub>2</sub>O<sub>3</sub> particles content, as it can be seen that Zn–ZnO–8Cr<sub>2</sub>O<sub>3</sub> displayed the optimum wear resistance, but the addition of Cr<sub>2</sub>O<sub>3</sub> in the matrix has immensely contributed to the wear resistance.

### Hardness property

With the Vickers microhardness tester, the microhardness/depth profiles for the Zn–ZnO coating and Zn–ZnO–Cr<sub>2</sub>O<sub>3</sub> composite samples tested before and after the heat treatment were plotted (Figures 7–9). The thermal deformations were observed at 250°C for 4 h, and mechanical responses of the coated samples were investigated. A good increase in the microhardness value was observed in the Zn–ZnO–Cr<sub>2</sub>O<sub>3</sub>

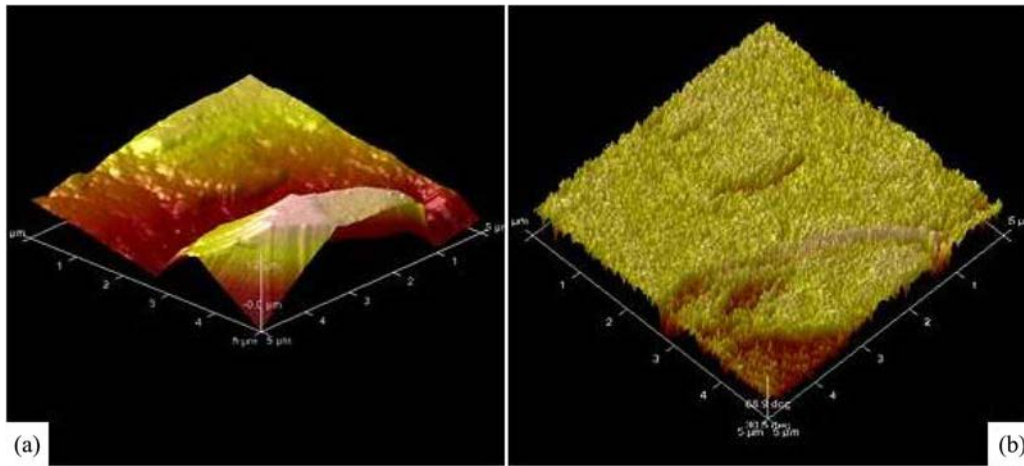


Figure 4. AFM of composite coating showing deposited surface topography and distribution: (a) Zn–8ZnO; and (b) Zn–8ZnO–16gCr<sub>2</sub>O<sub>3</sub>.

composite coating even before heat treatment, as shown in Figure 7a. The microhardness value for the Zn–ZnO material was 134.0 HVN and almost doubled for the Zn–8ZnO–8Cr<sub>2</sub>O<sub>3</sub> composite coating (which was the optimal performance) with a value of 344 HVN.

### Polarization measurements

The values of  $E_{\text{CORR}}$ ,  $j_{\text{CORR}}$ , corrosion rate (CR), and polarization resistance ( $R_p$ ) of the samples before heat treatment are extrapolated from Tafel slope as presented in Table 3. The results revealed the corrosion resistance behavior of the coatings in 3.65% NaCl static solution. From the polarization curves of Zn–ZnO–Cr<sub>2</sub>O<sub>3</sub> composite coating in Figure 10, it was found that the addition of Cr<sub>2</sub>O<sub>3</sub> altered the shape of the polarization curve but causes a considerable increase in the value of the  $E_{\text{corr}}$ .

### Discussion

The nature of the surface morphology and orientation in Figure 2 revealed the nonhomogeneous appearance but good discharges as expected. There are no pores and cracks at the interface, which shows that the interface bonding is firm. With reference to the work reported by Acharya and Upadhyay (2004), the distribution of the composite and iron adjacent

to the interface and their variation as a function of distance from the interface were apparent as seen in Figures 2 and 3. But the observed improvement may not be far from the possibility that the deposition behavior and the adhesion strength of any particular plating often based on the current density, potential, plating time, and strengthening effect of the grain present in the matrix (Umuru et al. 2006). In Figure 3, the increase in hardness may be attributed to the presence of Cr<sub>2</sub>O<sub>3</sub> in the matrix, particularly when the coating was induced below 12 g/L. Therefore, the dispersive strengthening effect and grain induced by ZnO/Cr<sub>2</sub>O<sub>3</sub> particulate orchestrated the improved performance as against the Zn–ZnO coating matrixes. One great characteristic of Zn–ZnO–Cr<sub>2</sub>O<sub>3</sub> in the presence of Cr<sub>2</sub>O<sub>3</sub> was the uniform and continuous thickness without any flaw. The absence of these defects and flaws along the interface is germane in this research and is a pointer of excellent coating and good adhesion properties.

Figure 4 revealed the morphology of the coating, indicating fine grain size, uniform arrangement, and crystal growth for the Zn–8ZnO–16gCr<sub>2</sub>O<sub>3</sub> coating, unlike the Zn–8ZnO deposition where good surface deposition was achieved but irregular or inhomogeneous dispersion of deposit was observed.

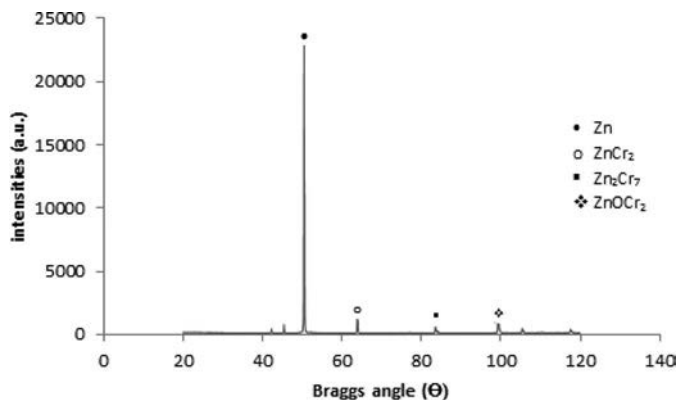


Figure 5. XRD patterns of the coating Zn–ZnO–Cr<sub>2</sub>O<sub>3</sub>.

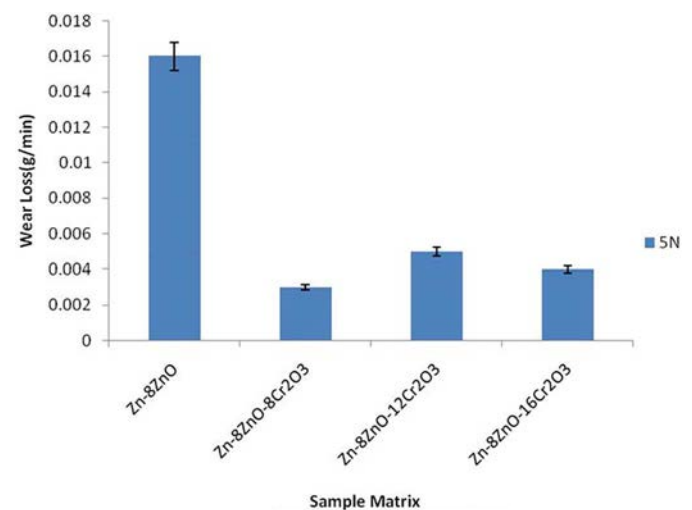
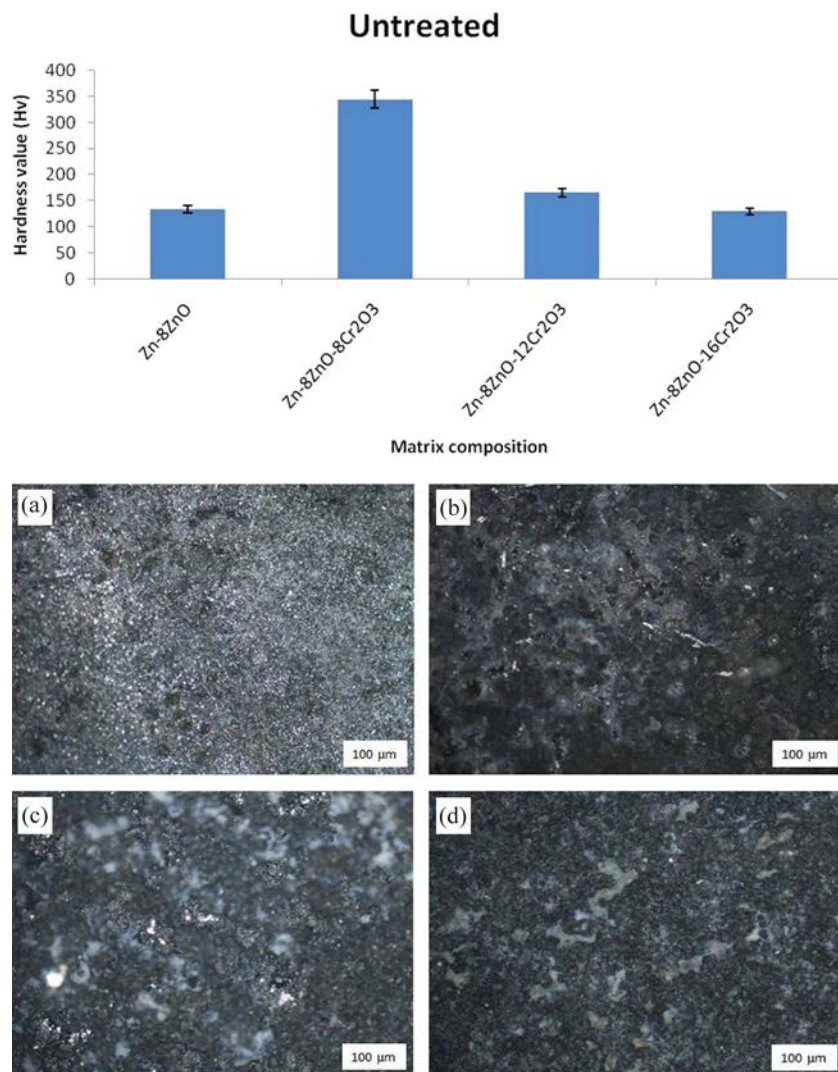


Figure 6. Variation of wear rate with time.



**Figure 7.** (Upper panel) Microhardness variation of the nanocomposite coating before being thermally induced. (Lower panel) Optical micrographs of the nanocomposite coating before being thermally induced: (a) Zn-8ZnO; (b) Zn-8ZnO-8Cr<sub>2</sub>O<sub>3</sub>; (c) Zn-8ZnO-12Cr<sub>2</sub>O<sub>3</sub>; (d) Zn-8ZnO-16Cr<sub>2</sub>O<sub>3</sub>.

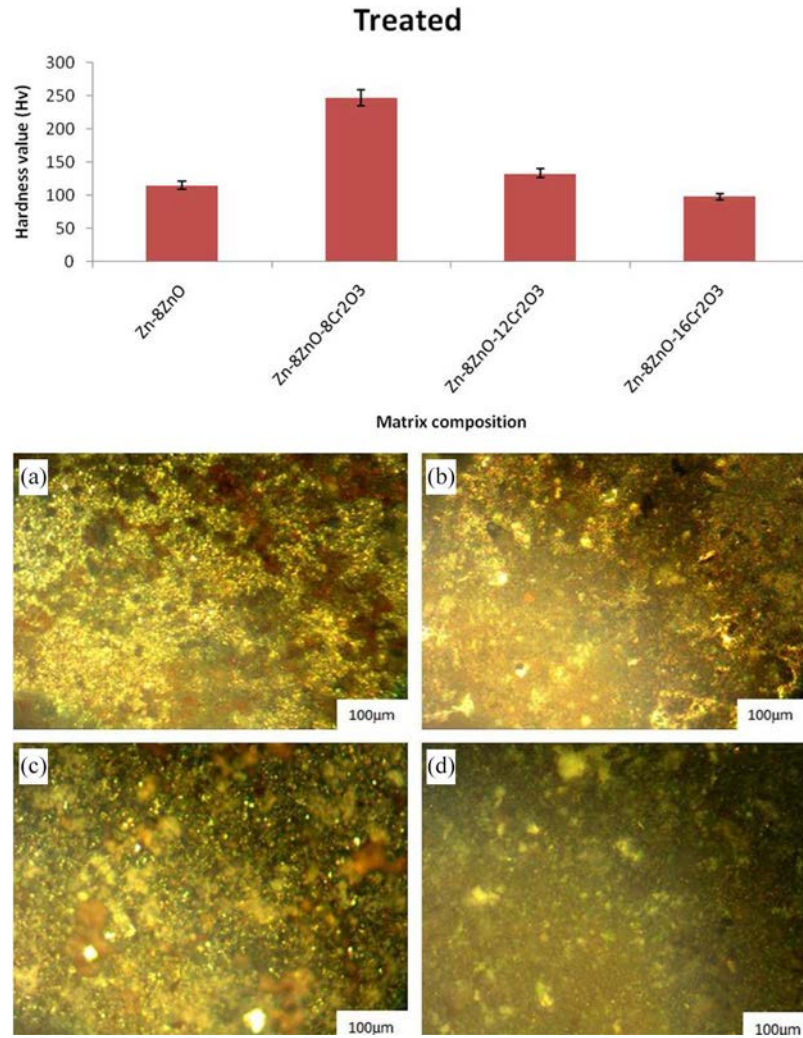
From the XRD result, the presence of the intermediate dispatched composite phases observed in Figure 5 could be traced by their inter-diffusion mechanism and ion of each particulate as reported by Khadom et al. (2009). The progressions of Zn hexagonal structure from all peaks of diffraction line were clearly visible in agreement with Khadom et al. (2009) and Oki et al. (2011). Therefore, the phase modification and new orientation of the metal matrix are clue of the performance and significant effect of the composites produced. This result was in concordance with studies carried out by Fustes et al. reported by Malatji et al. (2016), and zinc phase was seen at maximum peak level.

Figure 6 illustrates the wear analysis of the coatings. The improved wear resistance can be attributed to the strengthening effect. The hardness process parameter and microstructural behavior are the parameters which affect the wear resistance as indicated by Noor and Al-Moubaraki (2008). The wear resistance increases with increasing hardness of the matrix. The tendency of Zn-ZnO-Cr<sub>2</sub>O<sub>3</sub> composite coatings for plastic deformation is less than Zn-ZnO coating. The results suggest that the wear resistance was improved by the addition of Cr<sub>2</sub>O<sub>3</sub> particles. According to Popoola and Fayomi

(2011), the embedded Cr<sub>2</sub>O<sub>3</sub> particles can significantly improve the tribological performance of Zn-ZnO-Cr<sub>2</sub>O<sub>3</sub> composite coatings.

Figure 7a shows the microhardness variation of the nanocomposite coating before heat treatment. The increase in hardness of the Zn-ZnO-Cr<sub>2</sub>O<sub>3</sub> composite coated specimens is due to the presence of the Cr<sub>2</sub>O<sub>3</sub> as reinforcement additive, despite the fact that the increase in the quantity has limit. The optical micrographs of the coated samples before they were thermally induced are shown in Figure 7b.

Figure 8a revealed the response of the composite coating to the heat treatment. Although heating the samples did not increase their hardness property, the coating did not experience any crack or flaw at the interface. This can be seen in Figure 8b. In general, there is quite little reduction in hardness properties compared with the coated samples without heat treatment. The mechanical behavior due to thermal treatment and porosity within the alloy surface could result in hardness distribution. Some literatures also attested to the fact that compression stress could significantly improve the microhardness when it is much less than the ultimate strength of the coating. However, Paunovic and Mordechay (2006) discovered that the



**Figure 8.** (Upper panel) Microhardness variation of the thermally induced nanocomposite coating. (Lower panel) Optical micrographs of the nanocomposite coating after heat treatment: (a) Zn–8ZnO; (b) Zn–8ZnO–8Cr<sub>2</sub>O<sub>3</sub>; (c) Zn–8ZnO–12Cr<sub>2</sub>O<sub>3</sub>; (d) Zn–ZnO–16Cr<sub>2</sub>O<sub>3</sub>.

defect such as porosity and macro-particle at the alloy surface will have detrimental effect on the mechanical properties. [Figure 9](#) compares the hardness properties of the composite coatings before and after thermal treatment. The average microhardness values for all the samples calculated indicate that Zn–8ZnO–8Cr<sub>2</sub>O<sub>3</sub> possessed the highest hardness value of 344 HVN, though it decreased to 247 HVN after heat treatment but still maintained its optimal value. It should also be

noted that the coating was brilliant since the hardness values after heating were still maintained at more than 50% of their values before thermal treatment (Malatji et al. 2016). The phenomenon of dispersion strengthening was also observed. The mechanisms of such strengthening are the grain refinement strengthening and the dispersion strengthening of ZnO and Cr<sub>2</sub>O<sub>3</sub> deposited on the sample and the deposition current (Popoola and Fayomi 2011).

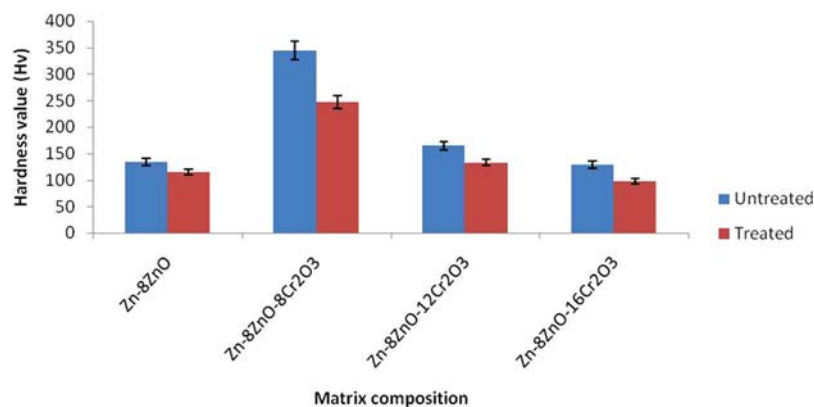


**Figure 9.** Microhardness variation of the nanocomposite coating before and after heat treatment.

**Table 3.** Polarization data extrapolated from Tafel slope for matrix Zn–ZnO–Cr<sub>2</sub>O<sub>3</sub> composite coating.

Samples	$E_{corr}$ , observations (V)	$j_{corr}$ (A/cm <sup>2</sup> )	CR (mm/year)	$R_p$ (Ω)
1. Zn–8ZnO	–1.3067	0.003029	0.854270	23.583
2. Zn–8ZnO–8Cr <sub>2</sub> O <sub>3</sub>	–1.1598	0.000115	0.025978	81.947
3. Zn–8ZnO–12Cr <sub>2</sub> O <sub>3</sub>	–1.2246	0.000130	0.033919	38.509
4. Zn–ZnO–16Cr <sub>2</sub> O <sub>3</sub>	–1.3706	0.003102	0.856890	20.390

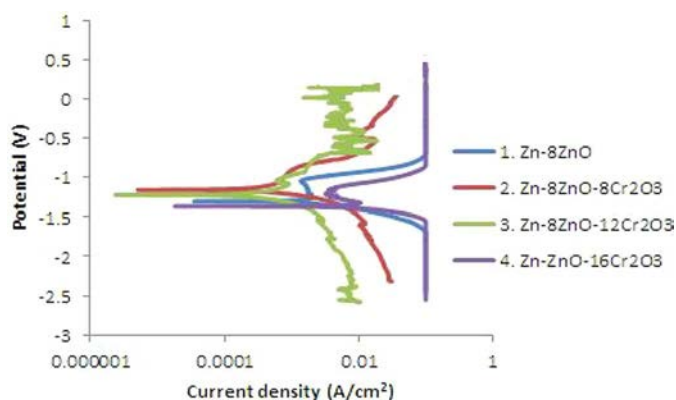


**Figure 10.** Potentiodynamic polarization curves of Zn–ZnO–Cr<sub>2</sub>O<sub>3</sub> composite coating on mild steel in 3.65% NaCl solution.

The features from the linear polarization test (Figure 10) indicate that an increase in additive concentration intensifies this process. However, the optimal value for the coating with least corrosion rate was for Zn–8ZnO–8Cr<sub>2</sub>O<sub>3</sub>, which implies that addition of Cr<sub>2</sub>O<sub>3</sub> gives better corrosion-resistant property. According to Ogundare et al. (2012), this could be attributed to the nature and tenacity of the passive film produced by Zn–8ZnO–8Cr<sub>2</sub>O<sub>3</sub> on the surface of the coated steel, and the drop in the potential thereafter could be traced to slight passivity breakdown experienced when

the concentration of Cr<sub>2</sub>O<sub>3</sub> was further increased, which is in line with Su and Kao (2003). Figure 11 shows corrosion morphologies of the composite coating after corrosion tests in the accelerated solution. Localized corrosion occurred on the surface of Zn–8ZnO and Zn–ZnO–16Cr<sub>2</sub>O<sub>3</sub> while the other alloys with Cr<sub>2</sub>O<sub>3</sub> show uniform corrosion on the surface. ZnO-rich intermetallic particles and excess Cr<sub>2</sub>O<sub>3</sub> globules are pit initiation sites and promote cathodic reduction reactions. The very low Linear Polarization Resistance (LPR) for both Zn–8ZnO and Zn–ZnO–16Cr<sub>2</sub>O<sub>3</sub> is due to pitting corrosion initiated from ZnO-rich and excess Cr<sub>2</sub>O<sub>3</sub> particles.

## Conclusions

The following conclusions were drawn from the study:

1. Composite coatings consisting Zn–ZnO and Zn–ZnO–Cr<sub>2</sub>O<sub>3</sub> particles were successfully prepared by means of an electrodeposition technique onto carbon steel substrates.
2. The plating of Zn with incorporation ZnO and Cr<sub>2</sub>O<sub>3</sub> in the coating was confirmed by the EDS and XRD.
3. The co-deposition of nano-sized Cr<sub>2</sub>O<sub>3</sub> particles in a metal deposit modified the surface morphology of the substrate.
4. The developed composite coating was mechanically and thermally stable.
5. The presence of Cr<sub>2</sub>O<sub>3</sub> particles in the matrix of the coating system increased adhesion, corrosion resistance, and microhardness of the surface compared with that of plain carbon steel.

## Funding

This material is based upon work supported financially by the National Research Foundation. The authors acknowledge the support from Surface Engineering Research Centre, (SERC) Tshwane University of Technology Pretoria, South Africa.

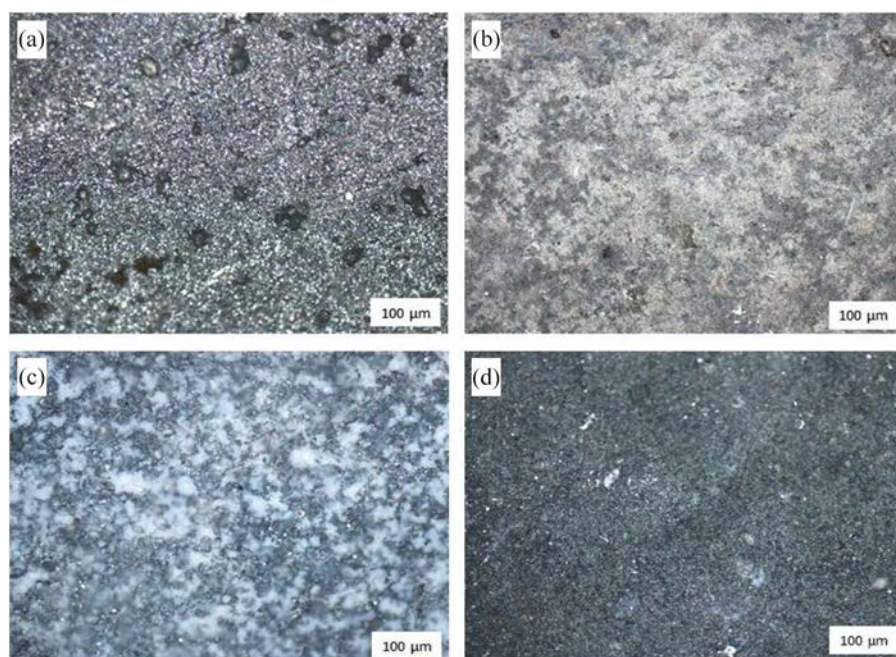


**Figure 11.** Optical micrographs of the nanocomposite coating after corrosion experiment: (a) Zn–8ZnO; (b) Zn–8ZnO–8Cr<sub>2</sub>O<sub>3</sub>; (c) Zn–8ZnO–12Cr<sub>2</sub>O<sub>3</sub>; (d) Zn–ZnO–16Cr<sub>2</sub>O<sub>3</sub>.

## References

- Acharya, S., and S. N. Upadhyay. 2004. The inhibition of corrosion of mild steel by some fluoroquinolones in sodium chloride solution. *Transactions of The Indian Institute of Metals* 57 (3):297–306.
- Burubai, W., and G. Dagogo. 2007. Comparative study of inhibitors on the corrosion of mild steel reinforcement in concrete. *Agricultural Engineering International* 9:1–10.
- Fayomi, O. S. I., A. P. I. Popoola, and V. S. Aigbodion. 2014. Effect of thermal treatment on the interfacial reaction, microstructural and mechanical properties of Zn–Al SnO<sub>2</sub>/TiO<sub>2</sub> functional coating alloys. *Journal of Alloys and Compounds* 617:455–463. doi:10.1016/j.jallcom.2014.07.141.
- Fayomi, O. S. I., V. R. Tau, A. P. I. Popoola, B. M. Durodola, O. O. Ajayi, C. A. Loto, and O. A. Inegbenebor. 2011. Influence of plating parameter and surface morphology on mild steel. *Journal of Materials and Environmental Science* 3:271–280.
- Harris, S. J., M. Mishon, and M. Hebbbron. 2006. Corrosion sensors to reduce aircraft maintenance. RTO AVT-144 Workshop on Enhanced Aircraft Platform Availability through Advanced Maintenance Concepts and Technologies, Vilnius, Lithuania.
- Khadom, A. A., A. S. Yaro, A. S. Altaie, A. H. Kadum, and A. Y. Musa. 2009. Mathematical modeling of corrosion inhibition behavior of low carbon steel in HCl acid. *Journal of Applied Sciences* 9:2457–2462. doi:10.3923/jas.2009.2457.2462.
- Malatji, N., A. P. I. Popoola, O. S. I. Fayomi, and C. A. Loto. 2016. Multifaceted incorporation of Zn–Al<sub>2</sub>O<sub>3</sub>/Cr<sub>2</sub>O<sub>3</sub>/SiO<sub>2</sub> nanocomposite coatings: Anti-corrosion, tribological, and thermal stability. *The International Journal of Advanced Manufacturing Technology* 82:1335–1341. doi:10.1007/s00170-015-7463-x.
- Munoz, A. I., J. G. Anton, S. L. Nuevalos, J. L. Guinon, and V. P. Herranz. 2004. Corrosion studies of austenitic and duplex stainless steels in aqueous lithium bromide solution at different temperatures. *Corrosion Science* 46 (12):2955–2974. doi:10.1016/j.corsci.2004.05.025.
- Noor, E. A., and A. H. Al-Moubaraki. 2008. Corrosion behavior of mild steel in hydrochloric acid solutions. *International Journal of Electrochemical Science* 3:806–818.
- Ogundare, O., B. Babatope, A. R. Adetunji, and S. O. O. Olusunle. 2012. Atmospheric corrosion studies of ductile iron and austenitic stainless steel in an extreme marine environment. *Journal of Minerals and Materials Characterization and Engineering* 11:914–918.
- Oki, M., E. Charles, C. Alaka, and T. K. Oki. 2011. Corrosion inhibition of mild steel in hydrochloric acid by Tannins Rom Rhizophora. *Materials Sciences and Applications* 2:592–595. doi:10.4236/msa.2011.26079.
- Paunovic, M., and S. Mordechay. 2006. *Fundamentals of electrochemical deposition*. vol. 6, 2nd ed., 388–391. New Jersey, USA: John Wiley and Son Inc.
- Popoola, A. P. I., O. S. I. Fayomi, and O. M. Popoola. 2012. Electrochemical and mechanical properties of mild steel electroplated with Zn–Al. *International Journal of Electrochemical Science* 7:4898–4917.
- Popoola, A. P. I., S. L. Pityana, and O. M. Popoola. 2011. Microstructure and corrosion properties of Al (Ni/TiB<sub>2</sub>) intermetallic matrix composite coatings. *Journal of the South African Institute of Mining and Metallurgy* 111:345–353.
- Rahman, M. J., S. R. Sen, M. Moniruzzaman, and K. M. Shorowordi. 2009. Morphology and properties of electrodeposited Zn–Ni Alloy coatings on mild steel. *Journal of Mechanical Engineering* 40 (1):9–14. doi:10.3329/jme.v40i1.3468.
- Shalaby, H. M., A. Al-Hashem, M. Lowther, and Al-Besharah. 1996. *Industrial Corrosion and Corrosion Control Technology* Kuwait Institute for Scientific Research, Kuwait.
- Shukla, S. K., A. K. Singh, and M. A. Quraishi. 2012. Triazines: Efficient corrosion inhibitors for mild steel in hydrochloric acid solution. *International Journal of Electrochemical Science* 7:3371–3389.
- Umoru, L. E., I. A. Fawehinmi, and A. Y. Fasasi. 2006. Investigation of the inhibitive influence of Theobroma cacao and cola acuminata leaves extracts on the corrosion of a mild steel in sea water. *Journal of Applied Sciences Research* 2:200–204.